

Contents lists available at ScienceDirect

Separation and Purification Technology

journal homepage: www.elsevier.com/locate/seppur



Correlation between particle deposition and the size ratio of particles to patterns in nano- and micro-patterned membrane filtration systems



Jun Hee Jang ^a, Jaewoo Lee ^a, Seon-Yeop Jung ^a, Dong-Chan Choi ^a, Young-June Won ^b, Kyung Hyun Ahn ^a, Pyung-Kyu Park ^{c,*}, Chung-Hak Lee ^{a,*}

- ^a School of Chemical and Biological Engineering, Seoul National University, Seoul 151-742, Republic of Korea
- ^b Center for Environment, Health and Welfare Research, Korea Institute of Science and Technology, Seoul 136-701, Republic of Korea
- ^cDepartment of Environmental Engineering, Yonsei University, 1 Yonseidae-gil, Wonju, Gangwon-do 220-710, Republic of Korea

ARTICLE INFO

Article history: Received 20 July 2015 Received in revised form 21 October 2015 Accepted 24 October 2015 Available online 26 October 2015

Keywords:
Patterned membrane
Nano-pattern
Nanoimprint lithography
Particle deposition
Surface topography

ABSTRACT

Recently, membrane surface patterning has attracted much attention as an innovative alternative to control membrane fouling that occurs with membrane filtration used in water and wastewater treatment. However, limited attention has been focused on patterned membranes with nano-scale features due to their difficult fabrication. As a result, there is a lack of research on membrane fouling by particle deposition occurring with a wide range of pattern sizes. In this study, we prepared patterned membranes with nano-scale hexagonally packed arrays using nanoimprint lithography as well as micro-scale patterned membranes. Filtration tests were conducted using the membranes in cross-flow ultrafiltration to demonstrate the effect of the size ratio of particles to membrane patterns on fouling by particle deposition on the membrane surface. We found that particle deposition was most efficiently mitigated by the patterned membranes when the size ratio was approximately 3. On the other hand, when the size ratio was much smaller than 3, particle deposition was significant and was nearly as much as that of nonpatterned membranes. In addition, when the size ratio was larger than 3, particle deposition increased with the increase in the size ratio. We explained the correlation between particle deposition and the size ratio of particles to membrane patterns in terms of shear stress near the surface of the membrane patterns using a computational fluid dynamics simulation technique. We anticipate that this study will provide a deeper understanding of the particle deposition phenomena in nano- and micro-patterned membrane filtration.

© 2015 Elsevier B.V. All rights reserved.

1. Introduction

Membrane processes for water and wastewater treatment have been extensively utilized over the past decades due to their benefits, including minimal required space of the plant, reliable quality of treated water, and effective disinfection [1–3]. However, the membrane processes still have a critical challenge of membrane fouling caused by colloids, organic compounds, and microorganisms. Membrane fouling is the primary cause of the increased operational and maintenance cost by deteriorating membrane performance and decreasing membrane life [4,5]. To alleviate the fouling problem, various studies have been conducted using biological [6,7], chemical [8], and physical [9] approaches. Among the studies, the control of surface topography has recently been introduced in membrane fabrication to reduce membrane fouling

by promoting shear stress and turbulence near the membrane surface [10]. Previous studies showed an increase in the critical flux due to superior anti-fouling properties of patterned membranes [11,12]. Culfaz et al. observed that micro-structured ultrafiltration (UF) hollow fiber membranes exhibited improvement in water flux, and their fouling reversibility was better than that of round fibers [13,14].

One interesting result reported by the previous studies is that foulants in a feed solution showed different deposition behavior according to their sizes under the condition of fixed pattern size [12,14]. In another case, the size and spacing of patterns were adjusted in accordance to the target organisms to prevent bacterial attachment and bio-fouling. The results indicated that the attachment of the bacterial cell was contingent on the feature dimensions [15–17].

To the best of our knowledge, however, no previous research on patterned membranes has investigated the effect of the correlation between sizes of foulants and membrane patterns on fouling

^{*} Corresponding authors.

E-mail addresses: pkpark@yonsei.ac.kr (P.-K. Park), leech@snu.ac.kr (C.-H. Lee).

mitigation over a wide range of membrane pattern sizes. Membranes with nano-scale patterns, up to a few hundred nanometers, have scarcely been investigated due to the difficulty in the fabrication of well-ordered nano-scale patterns on membrane surfaces. Gohari et al. prepared membranes with aligned nano-scale patterns by adding nanoparticles during a phase inversion process and demonstrated the importance of the orientation between surface patterns and feed flow direction on the fouling behavior [18]. However, the patterns used in their study were not sufficiently regular to distinctly clarify the effect of nano-scale patterns on fouling behavior. In addition, the study examined neither the comparison of the efficiency in fouling inhibition between patterned and flat membranes nor the influence of the interaction between foulant and pattern sizes on fouling behavior.

In this study, we prepared nano-patterned UF membranes using the nanoimprint lithography (NIL) method as well as micropatterned membranes to elucidate the impact of the size ratio of particles to membrane patterns on particle deposition. Anodized aluminum oxide (AAO), which is well known as a regular nanoporous material, was used as a mold to obtain well-ordered patterned features on the nano-scale. In addition, the relationship between membrane fouling and the ratio of particle to pattern size was investigated in a cross-flow filtration system by varying the particle and pattern sizes.

2. Materials and methods

2.1. Materials

An AAO mold with nano-scale patterns was prepared using high purity aluminum sheets (Al 99.999%, thickness ~0.5 mm, Goodfellow Inc., UK). Additionally, monoglycidyl ether-terminated poly (dimethylsiloxane) (MET-PDMS, Aldrich, USA) was used to make the surface of the mold hydrophobic. Polyurethane acrylate (PUA) molds with micro-scale patterns were prepared using silicon wafers ((100), p-type, Silicon Technology Co., Ltd., Japan), polydimethylsiloxane (PDMS, Sylgard 184 kit, Dow Corning, USA), polyethylene terephthalate (PET) film, polyurethane acrylate oligomer (PUA, Minuta Technology Co., Ltd., Republic of Korea), and sodium dodecyl sulfate (SDS, Sigma-Aldrich, USA). Polyethersulfone (PES, BASF, Germany) was used as a membrane material. N-methyl-2pyrrolidinone (NMP, Sigma-Aldrich, USA) was used as a solvent to prepare membranes. Glycerin (Duksan Pure Chemical, Republic of Korea) was utilized to prevent pore collapsing during the NIL process. The acids and organic solvents, including perchloric acid (HClO₄), oxalic acid (H₂C₂O₄), chromic acid (H₂CrO₄), hydrochloric acid (HCl), phosphoric acid (H₃PO₄), and ethanol, were purchased from Sigma-Aldrich, USA and were used without further purification. Aqueous suspensions of polystyrene latex microspheres (0.1, 0.5, 2, 5, and 6 µm in diameter, Alfa Aesar, USA) were utilized for colloidal filtration tests. Polycarbonate track-etched membranes with a pore diameter of 0.8 and 3 μm (Nuclepore[®], Whatman, GE Healthcare, USA) were purchased to separate mixed particles used in poly-dispersed particle filtration tests prior to determining each concentration.

2.2. Preparation of patterned molds for membrane fabrication

2.2.1. Nano-patterned mold

Nano-patterned AAO mold was prepared via a two-step anodization process [19] (Fig. 1). An aluminum sheet was prepared by electro-polishing in a mixed solution of ethanol and perchloric acid at 20 V and 4 $^{\circ}$ C to reduce surface roughness (Fig. 1a). Afterward, the electro-polished aluminum sheet was anodized in 0.3 M oxalic acid solution at 40 V and 15 $^{\circ}$ C for 12 h (Fig. 1b). After

the first anodization step, the nano-porous alumina layer was etched away with a mixture of chromic acid and hydrochloric acid at 65 °C (Fig. 1c). Subsequently, the second anodization was carried out under the same conditions as the previous anodization step except for an anodizing time of 100 s (Fig. 1d). To widen the AAO pore diameter, the porous AAO was immersed in 0.1 M phosphoric acid at 30 °C for 30 min (Fig. 1e). The porous AAO with a wider pore size was treated with MET-PDMS at 80 °C for 4 h to make its surface hydrophobic (Fig. 1f). The hydrophobic surface allows membranes to easily detach from the mold during membrane fabrication.

2.2.2. Micro-patterned mold

Concave dome-shaped micro-patterned PUA mold was prepared using the following procedure (Fig. 2). First, a hexagonally packed monolayer of particles on a silicon wafer was prepared via the self-assembling process [20]. A 2.5 wt% aqueous suspension of polystyrene latex particles with a diameter of 2 µm was diluted with a 4:1 (v/v) ethanol/polystyrene solution and was sonicated for 20 min to homogeneously disperse the particles. The diluted suspension (50 µL) was dropped onto deionized (DI) water to form a monolayer of the particles on the water surface. Then, a few drops of SDS were added to increase the rigidity of the particle monolayer. A piece of silicon wafer $(3 \text{ cm} \times 3 \text{ cm})$ treated with UV/O₃ as a hydrophilic surface treatment was immersed in the water. By drawing the silicon wafer as shown in Fig. 2a (scooping method), the hexagonally packed polystyrene particle monolayer was formed on the wafer surface and was dried at room temperature (Fig. 2b).

Next, concave dome-shaped micro-patterns were introduced using a pattern-transfer technique. The PDMS prepolymer mixture (10:1 (w/w) base/curing agent) was poured onto the dried particle monolayer array and was cured at 60 °C for 4 h (Fig. 2c). The solid-ified PDMS with concave patterns was removed, and the PUA mixture was cast onto it (Fig. 2d). The PET film was gently placed on the PUA layer as a support. The PUA polymer replica with convex patterns was cured under UV light ($\lambda = 360 \pm 20$ nm). Similarly, the micro-patterned PUA mold was obtained by repeating this replication using PUA, except using another wafer as the support of PUA instead of PET film (Fig. 2e). Finally, the concave dome-shaped micro-patterned PUA mold was obtained on the wafer support (Fig. 2f).

2.2.3. Non-patterned mold

A non-patterned PUA mold with a flat surface was prepared to fabricate non-patterned membranes as a control. A piece of silicon wafer was modified using UV/O₃ in advance and was treated with MET-PDMS to make a hydrophobic surface.

2.3. Preparation of patterned membranes using molds

A schematic procedure of the preparation of nano- or micropatterned PES membranes using the molds is depicted in Fig. 3. A PES membrane was prepared by the conventional non-solvent induced phase separation (NIPS) method. A polymer solution consisting of 15 wt% of PES and 85 wt% of NMP was cast onto fabric with a casting knife (Fig. 3a). By dipping the cast PES on the fabric in DI water, phase separation was induced (Fig. 3b). The solidified PES membrane was dehydrated by dipping the wet membrane into a 50 wt% glycerol aqueous solution for 24 h (Fig. 3c) and drying it at room temperature for 24 h to prevent the collapse of the pore structure during imprinting of the patterned mold onto membranes with heat [21]. Then, the patterning process was conducted using a hot-press machine (V-SYSTEM, Republic of Korea). A patterned (or non-patterned) mold prepared previously by the methods described in Section 2.2 was placed on the dried PES

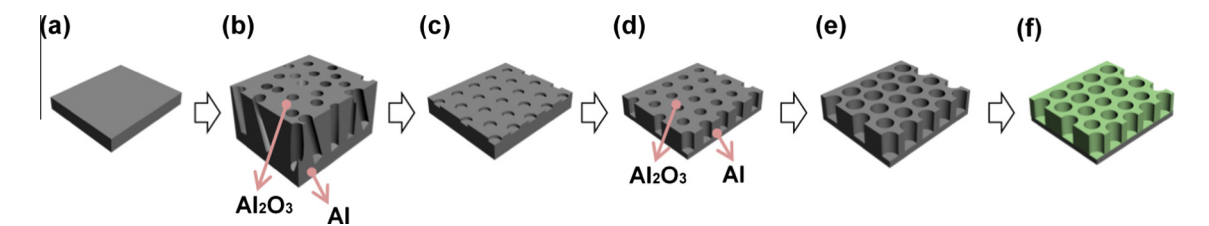


Fig. 1. Schematic procedure of preparing a nano-patterned anodized aluminum oxide (AAO) mold: (a) preparing electro-polished aluminum sheet, (b) the first anodization in oxalic acid, (c) etching the anodized aluminum sheet in a mixture of chromic acid and hydrochloric acid, (d) the second anodization in oxalic acid, (e) widening the pore size in phosphoric acid, and (f) hydrophobic treatment with a monoglycidyl ether-terminated poly(dimethylsiloxane) (MET-PDMS) solution.

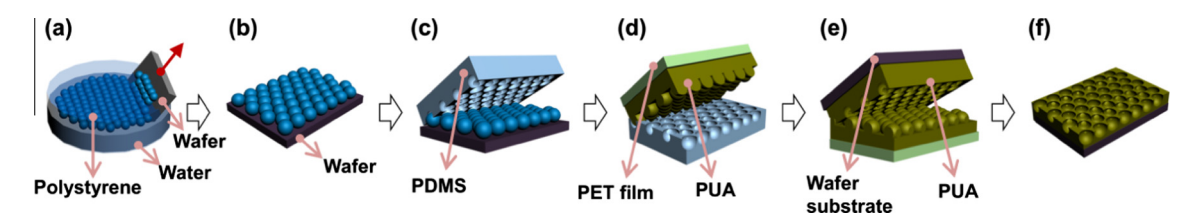


Fig. 2. Schematic procedure of preparing a micro-patterned polyurethane acrylate (PUA) mold: (a) forming a hexagonally packed polystyrene particle monolayer on a silicon wafer by drawing the wafer immersed in the water containing suspended polystyrene particles, (b) drying the monolayer on the wafer at room temperature, (c) transferring the patterns of the monolayer onto a PDMS substrate (concave patterns), (d) preparing a PUA replica with PET film (convex patterns) from the PDMS substrate under UV light for PUA curing, (e) transferring patterns onto another PUA layer with a silicon wafer (concave patterns), and (f) finally obtaining a concave dome-shaped micro-patterned PUA mold formed on a silicon wafer.

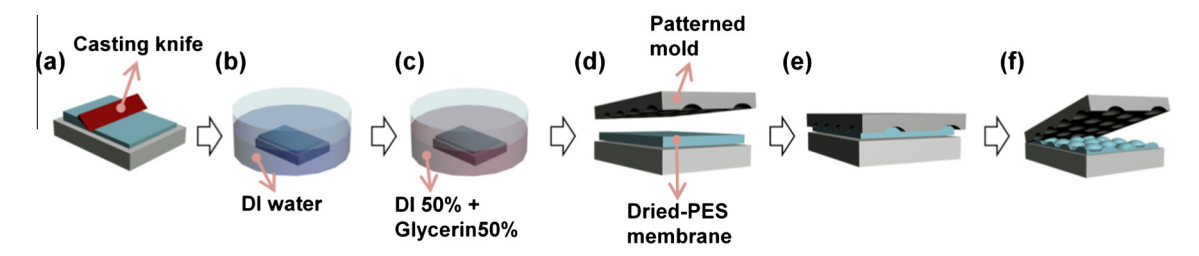


Fig. 3. Schematic procedure of preparing a nano- or micro-patterned polyethersulfone (PES) membrane (a) casting PES solution onto fabric with a casting knife, (b) dipping the casted PES on fabric in deionized water for non-solvent induced phase separation, (c) dipping the solidified PES membrane in 50 wt% glycerin aqueous solution and drying it, (d) placing a previously prepared patterned mold on the dried PES membrane, (e) transferring the patterns of the mold onto the PES membrane by pressing at 40 bar and 150 °C, (f) peeling off the patterned mold from the prepared PES membrane with nano- or micro-scale patterns.

membrane (Fig. 3d) and then was pressed at 40 bar and 150 °C for 5 min (Fig. 3e). After dipping the PES membrane with the mold into DI water at 20 °C, a patterned PES membrane was obtained after removing the mold (Fig. 3f). Prior to conducting membrane characterization and observing filtration performance, the prepared membranes were stored in DI water for 24 h.

2.4. Characterization of patterned membranes

The morphology of dried membranes was observed by atomic force microscopy (AFM, SPA300HV, NanoNavi, Seiko Instruments Inc., Japan) in the tapping mode and by scanning electron microscopy (SEM, JSM-6701F, JEOL, Japan) after platinum sputtering (Cressington 108 auto, Cressington Scientific Instruments Ltd., UK) onto the pieces of membranes. The pattern sizes of the membranes were estimated using freeware (Gwyddion) to visualize and analyze scanning probe microscopy data after the AFM measurement.

2.5. Filtration of particles using patterned membranes

2.5.1. Filtration of mono-dispersed particles

In particle filtration tests, a bench-scale cross-flow filtration system was used (Fig. S1 in supporting information). The volumetric flow rate of the retentate was to maintain a constant linear

velocity of 0.4 cm/s in the membrane module with a prepared membrane (Reynolds number = approximately 17). The diluted colloidal aqueous suspension of polystyrene latex microspheres with diameters of 0.1, 0.5, 2 or 6 µm was used as feed solution. The concentrations of feed solution corresponding to 0.1, 0.5, 2 and 6 µm were 1, 5, 20 and 20 ppm, respectively. The diluted feed suspensions were sonicated for 1 h prior to the filtration test to provide a thoroughly dispersed solution. Each membrane (i.e. nano-, micro- or non-patterned membranes) was compacted by filtrating DI water at 4 bar for 2 h, and then the mono-dispersed feed solution was filtered through each membrane for 2 h. To confirm the dispersion stability during the filtration test, the particle size in the feed reservoir was examined using electrophoretic light scattering spectrometry (ELS-Z2, Otsuka Electronic Co., Ltd., Japan) every 30 min. After completing each filtration test, the used membrane was immersed in DI water and was sonicated for 1 h to detach the particles deposited on the membrane. There was no significant change in the size of the particles detached from the membranes after sonication (Fig. S2 in supporting information). The total mass of detached particles was evaluated by measuring the absorbance of the particle solution with a spectrophotometer (OPTIZEN POP, Mechasys Co., Ltd., Republic of Korea). Because the wavelength corresponding to the maximum absorbance of the particle solution varied according to particle size, the absorbance of each particle solution was measured at wavelengths

ranging from 200 nm to 1000 nm every 50 nm (Fig. S3 in supporting information) to determine the optimal wavelength. At the optimum wavelength, the calibration curves between the concentration of the detached particle of each size in the suspension and its absorbance were obtained and are illustrated in Fig. S4 in supporting information. Using these calibration curves, the total mass of the particles deposited on the membrane could be calculated.

2.5.2. Filtration of poly-dispersed particles

The mixture of mono-dispersed particles with sizes of 0.5, 2 and 5 μ m (1:4:4 w/w/w) was diluted with DI water at a total concentration of 20 ppm to prepare a poly-dispersed suspension. Filtration of the suspension was carried out under the same conditions as the previous filtration test using mono-dispersed suspensions. After filtration, the particles deposited on the membranes were detached and dispersed by sonication for 1 h. To exclusively quantify the different types of detached particles according to particle size, size exclusion was performed using the track-etched membranes. The separated particles were detached from the track-etched membranes and re-dispersed in DI water. The total deposited mass of each particle was estimated and compared to evaluate particle deposition behavior according to the particle size of the poly-dispersed particles.

2.6. Numerical method

The two-dimensional simulation performed in this study is similar to that described in a previous study [10]. Briefly, we assumed the fluid to be a steady-state incompressible Newtonian fluid to simplify the calculation with a density of 10^3 kg/m 3 and a viscosity of 10^{-3} kg/(m s). The following Navier–Stokes and continuity equations were solved to analyze the flow behavior near the patterned membrane surface:

$$\rho(\mathbf{u}\nabla)\mathbf{u} = \nabla[-p\mathbf{I} + \eta(\nabla\mathbf{u} + (\nabla\mathbf{u})^T)] \tag{1}$$

$$\nabla \mathbf{u} = 0 \tag{2}$$

where **u** is the velocity vector of the fluid, p is the pressure, ρ is the density of the fluid, and η is the viscosity of the fluid [10].

Commercial software, COMSOL Multiphysics (COMSOL 3.2, Comsol Inc., USA), was utilized to conduct this flow analysis.

We also employed the geometry to simulate the size and shape of the membranes used in the experiments (Fig. S5 in supporting information). The overall simulation domains had a width of $10~\mu m$ and a height of $5~\mu m$ for each membrane. Only the regions near the membrane surface were considered in this flow analysis to focus on the flow characteristics near the surface patterns. Triangular elements were utilized to construct computational meshes, resulting in 30,178, 16,690 and 11,250 meshes for nano, micro- and non-patterned membranes, respectively.

A fully developed velocity profile for the Newtonian fluid was imposed as the inlet boundary condition. The maximum inlet velocity was set to 6 mm/s, which corresponds to 1.5 times the mean linear velocity in the experiments. On the upper boundary, a fully developed velocity profile for the Newtonian fluid was also applied with the assumption that flow perturbation in the presence of the surface patterns could be neglected. On the membrane surface, a no-slip boundary condition was imposed. At the outlet, atmospheric pressure (open to atmosphere, p = 0) was applied as a pressure boundary condition.

Back-transport velocities related to the lift forces induced by Brownian diffusion, shear induced diffusion, lateral migration due to fluid inertia, and charge repulsion were calculated in the Fig. S6 in supporting information. It was confirmed that all the particles with a diameter of 0.1, 0.5, 2 and 6 μ m used in this study would be well deposited without the effect of patterns.

3. Results and discussion

3.1. Preparation of patterned membranes

Fig. 4 shows membrane top-surface images and cross-sectional profiles obtained using AFM. Non-patterned membranes have a relatively smoother surface with <4 nm of variation in height (Fig. 4a), whereas nano- and micro-patterned membranes have nano- and micro-scaled hexagonal packing patterns on their surfaces, respectively (Fig. 4b and c). This is because all of the patterned molds had well-ordered hexagonal packing arrays,

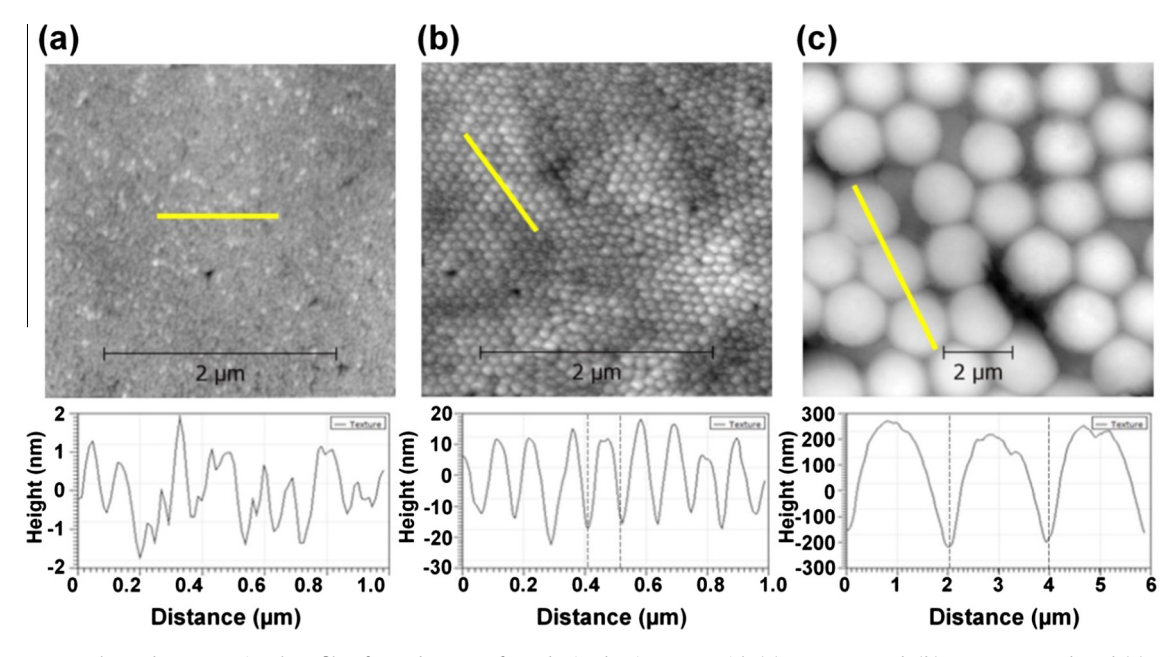


Fig. 4. Surface topography and cross-sectional profile of membrane surface obtained using AFM with (a) non-patterned, (b) nano-patterned, and (c) micro-patterned membranes.

regardless of pattern sizes (Fig. S7 in supporting information). In this study, the pattern size was defined as the width of each convex dome-shaped pattern. According to the AFM images and the corresponding cross-sectional profiles, each pattern size of nano- and micro-patterned membranes was approximately 0.1 and 2 μm , respectively (Fig. 4b and c).

The intrinsic water permeabilities of non-patterned and patterned membranes were calculated using surface areas considering pattern surface areas and were not significantly different from each other, which is described further in supporting information with Table S1.

3.2. Deposition behavior of mono-dispersed particles on the patterned membranes

After the cross-flow filtration of mono-dispersed colloidal suspensions at the Reynolds number of approximately 17 for 1 h, the mass of particles deposited on each membrane was estimated using a spectrophotometer and the calibration curves previously mentioned. Fig. 5 shows the total data for the mass of the particles deposited on the membrane surface per unit membrane area.

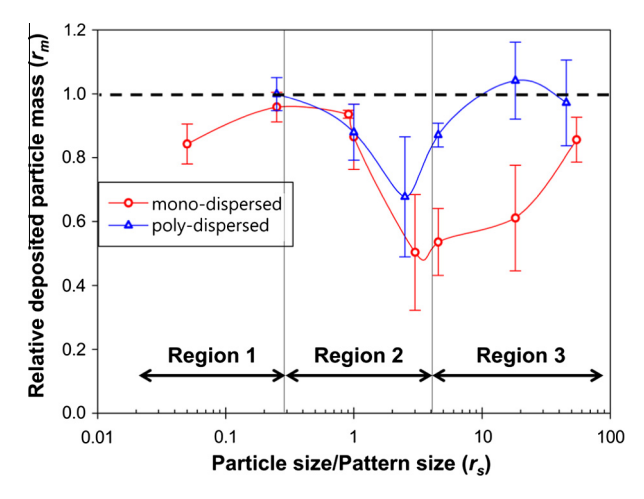


Fig. 6. Change in relative deposited particle mass (r_m) as a function of the size ratio of particle to pattern (r_s) appearing in the filtration test using mono-dispersed feed $(0.1, 0.5, 2, \text{ or } 6 \ \mu\text{m})$ particles) and poly-dispersed feed (mixture of 0.5, 2, and 5 μ m particles) (n = 2).

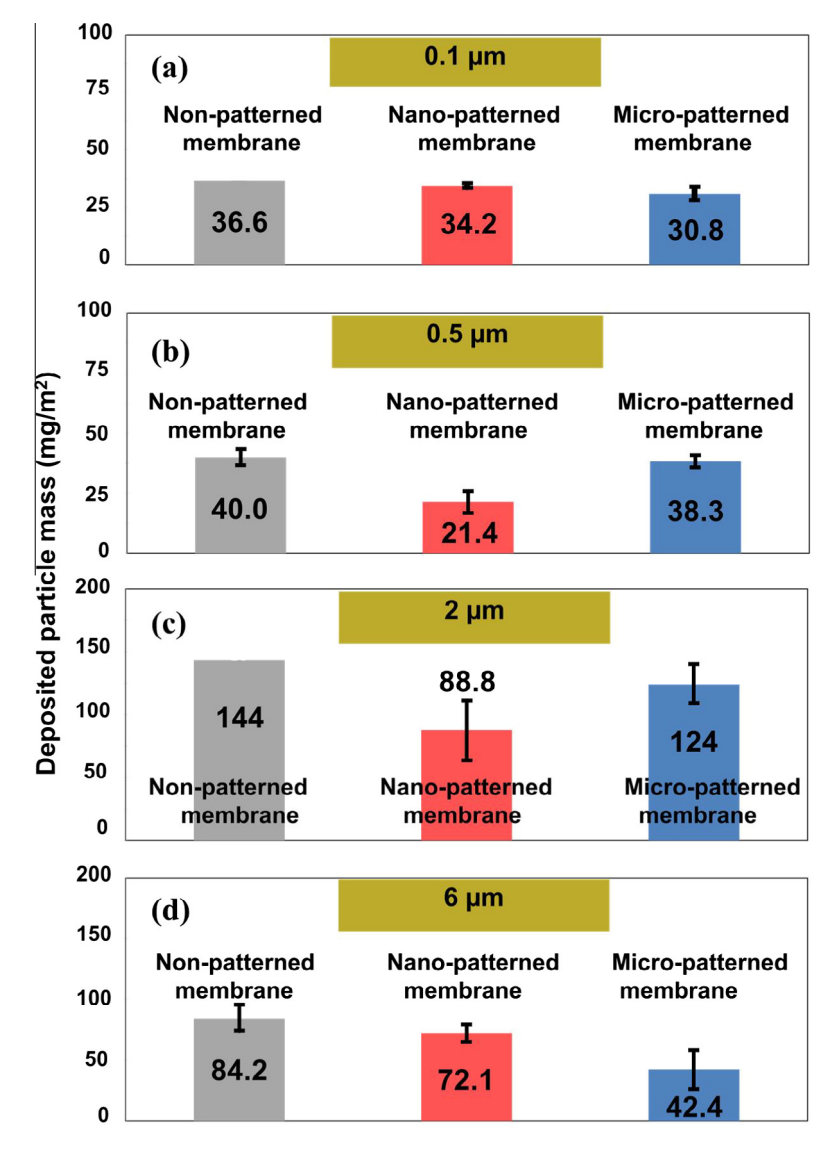


Fig. 5. The mass of particles deposited on each membrane after cross-flow filtration using (a) 0.1, (b) 0.5, (c) 2, and (d) 6 μm-sized particles (n = 2).

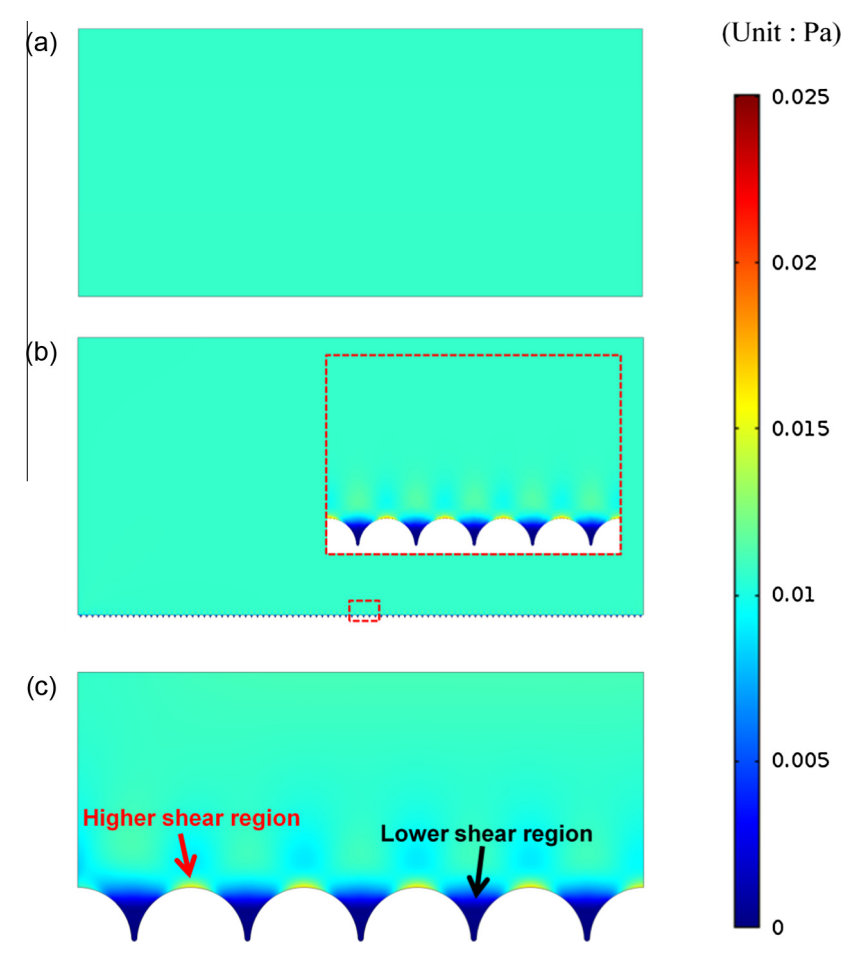


Fig. 7. Simulated shear stress near the surface of (a) non-patterned, (b) nano-patterned, and (c) micro-patterned membranes.

Comparing the mass of particles deposited on the patterned membranes with that on non-patterned membranes, the effect of patterns on particle deposition was variable with respect to particle size. There was no significant difference in particle deposition between non-patterned and patterned membranes in colloidal particle filtration using 0.1 μm particles (Fig. 5a). In colloidal particle filtration using 0.5 and 2 μm particles, however, the fewest particles were deposited on the nano-patterned membrane than on the micro- and non-patterned membranes. On the other hand, 6 μm particles tended to deposit more on nano- and non-patterned membranes than on the micro-patterned membrane (Fig. 5d). Overall, it was difficult to determine a clear explanation of the effect of patterns on particle deposition in terms of the sizes of the patterns and particles based on Fig. 5.

To clarify the effect of pattern and particle sizes, we examined the relative deposited particle mass according to the size ratio between the particle and pattern (Fig. 6). The relative deposited particle mass, r_m , and the size ratio of particle to pattern, r_s , are defined as follows:

Relative deposited particle mass (r_m)

$$= \frac{\text{deposited particle mass on patterned membrane}}{\text{deposited particle mass on non-patterned membrane}}$$
 (3)

Size ratio of particle to pattern
$$(r_s) = \frac{\text{particle size}}{\text{pattern size}}$$
 (4)

When the particle deposition is reduced by the introduction of a pattern, for instance, r_m is less than 1 for patterned membranes. A small value of r_s indicates that the particle size is small compared to the pattern size.

The values of r_m and r_s were calculated from the data in Fig. 5 for the mono-dispersed particle filtration test and are plotted in Fig. 6. From the plot, the correlation between r_m and r_s was divided into three regions along with the r_s values: Below an r_s value of 0.3 (Region 1 in Fig. 6), r_m is close to 1, indicating that there is virtually no discernible difference in the anti-fouling property between non-patterned and patterned membranes. When r_s is larger than 0.3 and the particle size becomes comparable to the pattern size (Region 2 in Fig. 6), however, r_m begins to decrease to 0.5 at r_s = 3 (particle size = 6 μ m and pattern size = 2 μ m), indicating that the particle deposition on the patterned membrane was reduced to half that of the non-patterned membrane due to the anti-fouling effect of the patterns. As r_s exceeds 3, r_m increased toward 1 and the anti-fouling effect of patterns might be diminished (Region 3 in Fig. 6).

These findings in terms of r_m vs r_s were interpreted by simulating shear stress near the membrane surface. The effect of shear stress induced by a surface pattern can vary with pattern position. Lee et al. reported that local wall shear stress in the upper region of the pattern is higher than that in the lower region [10]. Our simulation result performed with a dome-shaped patterned membrane system is also in accordance with the previous study on the shear stress distribution to mitigate the fouling in the patterned membrane system regardless of pattern size (Fig. 7).

The lower shear regions in Fig. 7b and c for patterned membranes are located between dome-shaped patterns. In other words, the lower region corresponding to a valley between patterns induces a smaller shear stress, making it difficult for particles much smaller than the pattern size (*Region* 1) to detach from membranes once deposited in valleys. To confirm the deposition

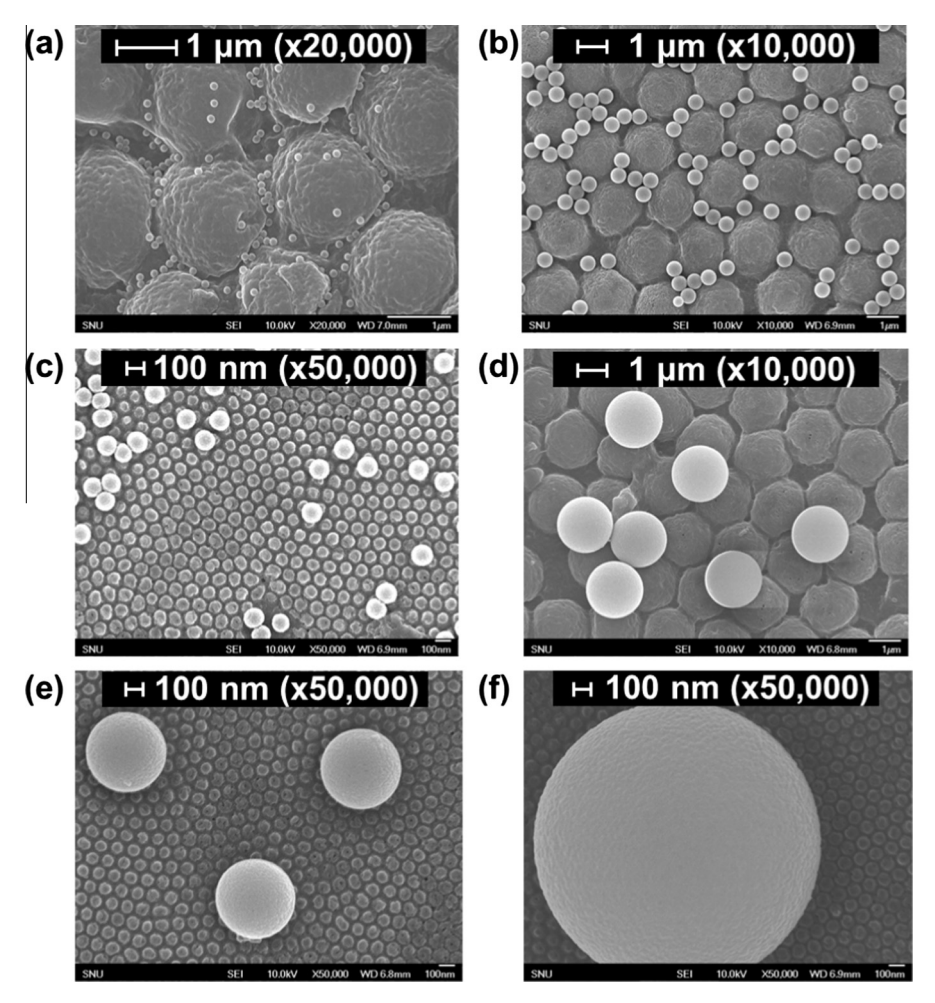


Fig. 8. SEM images of deposited particles on patterned membrane surfaces. (a) 0.1 μm particles on a micro-patterned membrane, (b) 0.5 μm particles on a micro-patterned membrane, (c) 0.1 μm particles on a nano-patterned membrane, and (f) 2 μm particles on a nano-patterned membrane.

tendency of smaller particles on the patterned membranes in *Region* 1, the SEM images of particles on the patterns were examined (Fig. 8).

Most particles with a size of 0.1 um were mainly deposited in the valley between 2 um micro-patterns, whereas the upper regions were sparsely fouled (Fig. 8a). This suggests that the effect of the patterns on particle detachment could be too small to detach particles from the membrane surface due to the lower shear stress in valleys under the Region 1 condition. Moreover, particles with a size comparable to valley region can be trapped. Once particles are trapped, it is difficult to detach the trapped particles from the membrane surface. According to a previous study [22], foulants with a similar size to the spacing between patterns were able to fit into the spacing, which caused the foulants to remain in the spacing. Similarly, a number of 0.5 µm particles were located in a low shear region and were trapped between the 2 micro-sized patterns as shown in Fig. 8b. From these phenomena, the fouling of the patterned membrane in Region 1 is attributed to the deposition in the low shear stress region and the trapping between patterns.

Unlike *Region* 1, the particle deposition was well mitigated in *Region* 2. In this region, it is physically impossible for particles to be placed in the lower shear region and to be trapped between patterns because the size of the particles is larger than the valley or spacing between patterns. Therefore, the particles could deposit only on the upper or top position of dome-shaped patterns

(Fig. 8c and d). The particles deposited on upper parts of patterns could be easily detached by high shear stress near the peaks of the patterns (Fig. 7b and c), thus, increasing the anti-fouling property of patterned membranes, as shown in *Region* 2 in Fig. 6.

An r_s larger than 0.3 (Region 3) is not desirable to enhance the anti-fouling effect compared with the non-patterned membrane, as shown in Fig. 6. Particle deposition on patterned membranes was also confirmed by SEM analysis (Fig. 8e and f). The particle deposition on non-patterned and patterned membranes was similar to each other. In Fig. 9, shear stress on nano- patterned membrane was represented with 0.1, 0.5, 2 and 6 µm particles. The sizes of patterns in Fig. 9 are all the same, but the magnification of Fig. 8a-d was changed to draw particles with different sizes. For large particles corresponding to Region 3, shear stress induced by patterns (the yellow parts near the top of dome-shaped patterns) could not be significant to the particles. Especially for the case depicted in Fig. 8d, shear stress appears to have an almost equal effect on the reduction of particle deposition or the detachment of deposited particles to that of a non-patterned flat surface, making r_m close to 1. This is responsible for the re-bound of the r_m value as the r_s value transits from Region 2 to Region 3.

These results suggest that an optimum value of r_s was approximately 3 for the inhibition of particle deposition in this study. Although it is difficult to quantitatively assess the balancing effects

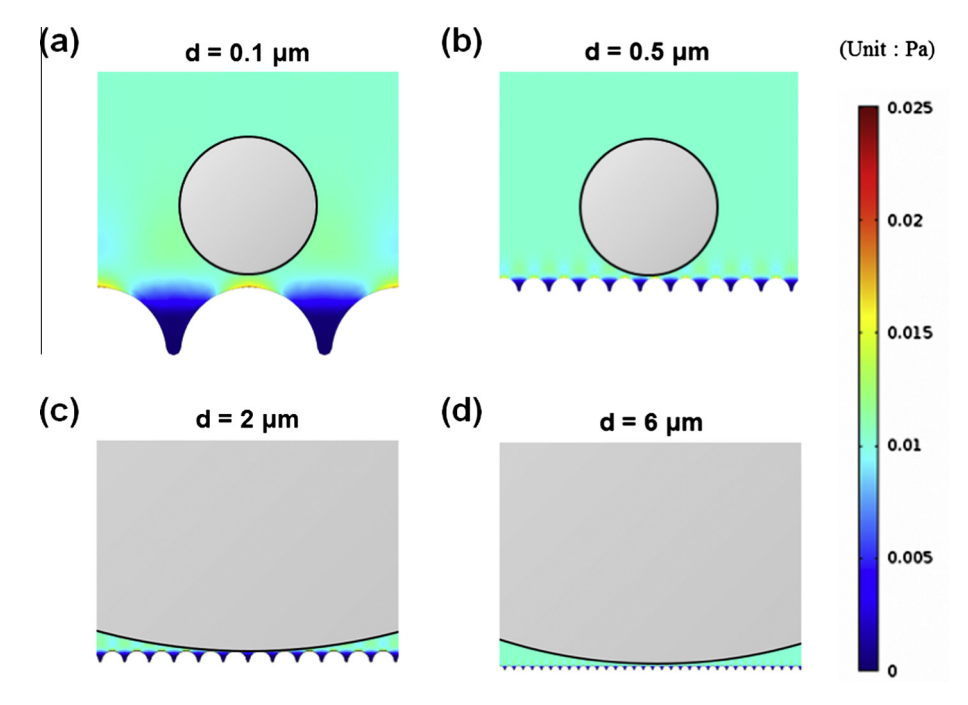


Fig. 9. Simulated shear stress occurring on nano-patterned membrane surface with (a) 0.1 µm, (b) 0.5 µm, (c) 2 µm, and (d) 6 µm particles.

of particle and pattern sizes, the obtained results indicate that the dominant factor affecting particle deposition depends on the size ratio of particle to pattern, r_s .

3.3. Deposition behavior of poly-dispersed particles on the patterned membranes

Most real systems contain numerous sizes of foulants, which are almost never mono-dispersed. Therefore, it is necessary to conduct a filtration test using a poly-dispersed feed solution. In this study, we carried out cross-flow filtration tests using a mixture composed of three different sizes of particles (0.5, 2, and 5 μm) under the same conditions as the mono-dispersed particle filtration. The composition of the poly-dispersed particle mixture in the feed tank was not significantly changed (<0.5%) in spite of the particle deposition because the amount of particles in the mixture was sufficient. Therefore, the size distribution of retentate returned back to the feed tank was regarded as almost the same as that of the initial feed solution.

The $r_{\rm m}$ and $r_{\rm s}$ for poly-dispersed particle experiments were calculated using the deposited masses of particles with each size (0.5, 2, and 5 µm) separated using track-etched membranes and the individual diameters of particles in the mixture. The correlation between r_m and r_s in the poly-dispersed system is similar to that in the mono-dispersed system as shown in Fig. 6. Therefore, the explanation on the mono-disperse case could be applied. Three different types of particle depositions could appear simultaneously, depending on the r_s in the patterned membrane system using poly-dispersed particles. For particles much smaller than the patterns in the particle mixture (Region 1), there was no significant mitigation in particle deposition by the introduction of a pattern. which resulted from the deposition in the lower shear region and particle trapping. For particles having r_s values from 0.3 to 3 (Region 2), the particle deposition on patterned membranes was less than that on non-patterned membranes due to physical constraints, and the shear effect induced by patterns became more prominent, thus alleviating fouling by particle deposition. For large particles with values of $r_s > 3$ in the particle mixture (*Region* 3), the difference between the deposition behaviors of non-patterned and patterned membranes decreased as the particle size became much larger than the pattern size. Overall, for both of the mono-dispersed and poly-dispersed particle solutions, particle deposition phenomena could be properly understood in terms of the ratio of particle to pattern size.

4. Conclusion

Nano- and micro-scaled (approximately 0.1 μm and 2 μm, respectively) hexagonal packing patterns were successfully applied to UF membranes. The mutual effect of pattern and particle sizes on particle deposition was examined by performing a colloidal filtration test using various sizes of latex particles. According to the analysis of the relationship between the relative deposited particle mass (deposited particle mass on patterned membranes divided by that on non-patterned membranes) and the size ratio of particles to patterns, we confirmed that there is an optimum size ratio in a patterned membrane filtration system. This optimum ratio appears when the particle deposition is not governed by deposition in a lower shear region and by particle trapping between patterns but by pattern effects, including shear stress induced by patterns. Finally, the individual behavior of particles in the mixture consisting of several sizes of particles is similar to that in a monodispersed solution. Although the absolute optimized size ratio can vary with the operating conditions of the filtration test and the features of patterns such as pattern shape, this study shows the probability that there may be an optimum size ratio of particles to membrane patterns for preventing particle deposition and that an appropriate pattern size can be chosen to maximize the resistance to particle deposition.

Acknowledgements

This work was supported by the National Research Foundation of South Korea Grant funded by the Korean Government (MEST) (NRF-2010-C1AAA001-0029061).

Appendix A. Supplementary material

Supplementary data associated with this article can be found, in the online version, at http://dx.doi.org/10.1016/j.seppur.2015.10.

References

- S. Adham, P. Gagliardo, L. Boulos, J. Oppenheimer, R. Trussell, Feasibility of the membrane bioreactor process for water reclamation, Water Sci. Technol. 43 (2001) 203–209.
- [2] H. Van der Roest, D.P. Lawrence, A. Van Bentem, Membrane bioreactors for municipal wastewater treatment, (2005).
- [3] J. Lee, H.-R. Chae, Y.J. Won, K. Lee, C.-H. Lee, H.H. Lee, I.-C. Kim, J.-M. Lee, Graphene oxide nanoplatelets composite membrane with hydrophilic and antifouling properties for wastewater treatment, J. Membr. Sci. 448 (2013) 223–230.
- [4] J. Baker, L. Dudley, Biofouling in membrane systems—a review, Desalination 118 (1998) 81–89.
- [5] E.M. Vrijenhoek, S. Hong, M. Elimelech, Influence of membrane surface properties on initial rate of colloidal fouling of reverse osmosis and nanofiltration membranes, J. Membr. Sci. 188 (2001) 115–128.
- [6] K.-M. Yeon, W.-S. Cheong, H.-S. Oh, W.-N. Lee, B.-K. Hwang, C.-H. Lee, H. Beyenal, Z. Lewandowski, Quorum sensing: a new biofouling control paradigm in a membrane bioreactor for advanced wastewater treatment, Environ. Sci. Technol. 43 (2008) 380–385.
- [7] H.-S. Oh, K.-M. Yeon, C.-S. Yang, S.-R. Kim, C.-H. Lee, S.Y. Park, J.Y. Han, J.-K. Lee, Control of membrane biofouling in MBR for wastewater treatment by quorum quenching bacteria encapsulated in microporous membrane, Environ. Sci. Technol. 46 (2012) 4877–4884.
- [8] K. Kim, K. Lee, K. Cho, C. Park, Surface modification of polysulfone ultrafiltration membrane by oxygen plasma treatment, J. Membr. Sci. 199 (2002) 135–145.
- [9] İ.S. Ngene, R.G. Lammertink, M. Wessling, W.G. Van der Meer, Particle deposition and biofilm formation on microstructured membranes, J. Membr. Sci. 364 (2010) 43–51.

- [10] Y.K. Lee, Y.-J. Won, J.H. Yoo, K.H. Ahn, C.-H. Lee, Flow analysis and fouling on the patterned membrane surface, J. Membr. Sci. 427 (2013) 320–325.
- [11] Y.-J. Won, J. Lee, D.-C. Choi, H.R. Chae, I. Kim, C.-H. Lee, I.-C. Kim, Preparation and application of patterned membranes for wastewater treatment, Environ. Sci. Technol. 46 (2012) 11021–11027.
- [12] S.H. Maruf, L. Wang, A.R. Greenberg, J. Pellegrino, Y. Ding, Use of nanoimprinted surface patterns to mitigate colloidal deposition on ultrafiltration membranes, J. Membr. Sci. 428 (2013) 598–607.
- [13] P.Z. Çulfaz, E. Rolevink, C. van Rijn, R.G. Lammertink, M. Wessling, Microstructured hollow fibers for ultrafiltration, J. Membr. Sci. 347 (2010) 32–41
- [14] P.Z. Çulfaz, S. Buetehorn, L. Utiu, M. Kueppers, B. Bluemich, T. Melin, M. Wessling, R.G. Lammertink, Fouling behavior of microstructured hollow fiber membranes in dead-end filtrations: critical flux determination and NMR imaging of particle deposition, Langmuir 27 (2011) 1643–1652.
- [15] M.V. Graham, N.C. Cady, Nano and microscale topographies for the prevention of bacterial surface fouling, Coatings 4 (2014) 37–59.
- [16] J.F. Ling III, M.V. Graham, N.C. Cady, Effect of topographically patterned poly (dimethylsiloxane) surfaces on pseudomonas aeruginosa adhesion and biofilm formation, Nano Life 2 (2012), http://dx.doi.org/10.1142/ S1793984412420044.
- [17] S.D. Puckett, E. Taylor, T. Raimondo, T.J. Webster, The relationship between the nanostructure of titanium surfaces and bacterial attachment, Biomaterials 31 (2010) 706–713.
- [18] R.J. Gohari, W.T. Lau, T. Matsuura, A.F. Ismail, Effect of surface pattern formation on membrane fouling and its control in phase inversion process, J. Membr. Sci. 446 (2013) 326–331.
- [19] H. Masuda, K. Fukuda, Ordered metal nanohole arrays made by a two-step replication of honeycomb structures of anodic alumina, Science 268 (1995) 1466–1468.
- [20] J.R. Oh, J.H. Moon, S. Yoon, C.R. Park, Y.R. Do, Fabrication of wafer-scale polystyrene photonic crystal multilayers via the layer-by-layer scooping transfer technique, J. Mater. Chem. 21 (2011) 14167–14172.
- [21] P.G. Bansod, V. Sapkal, R. Sapkal, Influence of ethanol concentration on the performance of polyethersulfone ultra filtration membranes, Int. J. ChemTech Res. 4 (2012) 1518–1521.
- [22] K.A. Whitehead, J. Verran, The effect of surface topography on the retention of microorganisms, Food Bioprod. Process. 84 (2006) 253–259.